Phys Chem Minerals (2003) 30: 157–166
DOI 10.1007/s00269-003-0299-1

ORIGINAL PAPER

S. Webb · I. Jackson

Anelasticity and microcreep in polycrystalline MgO at high temperature: an exploratory study

Received: 11 April 2002 / Accepted: 9 January 2003

Abstract The frequency dependence of the shear modulus and dissipation in polycrystalline MgO has been determined at high temperature using both microcreep ($\varepsilon = 10^{-4}$) and seismic frequency forced-oscillation ($\varepsilon = 10^{-5}$) measurements. The frequency-dependent and time-dependent data have been described in terms of the elastic, anelastic and viscous components of deformation using the Andrade model. The forced-oscillation measurements show that for temperatures above 700 °C the shear modulus begins to decrease dramatically and the modulus becomes frequency-dependent with increasing temperature. This is accompanied by an increase in dissipation, which also becomes frequency-dependent. The microcreep measurements resolve this frequency-dependent behaviour into an anelastic regime from 700–1050 °C, and a viscoelastic regime from 1100–1300 °C. At 1300 °C, the seismic frequency shear wave speed is ~60% of the extrapolated low-temperature frequency-independent value, and the dissipation has risen to $Q^{-1} = 10^{-1}$ from 10^{-3} at temperatures below 600 °C. The mechanism by which this frequency-dependent rheology occurs appears to be diffusional creep, which produces viscous slip on the grain boundaries. It is proposed that the anelastic behaviour is due to viscous slip occurring on segments of grain boundaries, with the viscous deformation being accommodated by elastic distortion of adjacent unslipped regions of the grain boundary. At higher temperatures, slippage occurs across the entire grain boundary and viscoelastic behaviour begins to occur.

S. Webb (✉) · I. Jackson
Research School of Earth Sciences,
Institute of Advanced Studies,
Australian National University,
Canberra ACT, Australia
e-mail: swebb@gwdg.de

S. Webb
Experimentelle und Angewandte Mineralogie,
Geowissenschaftliches Zentrum Göttingen,
Georg-August-Universität, Göttingen, Germany

Keywords Viscoelasticity · MgO · Anelasticity · Seismic frequency · Forced oscillation · Micro-creep

Introduction

The energy of a propagating wave can be absorbed by various physical processes within a crystalline material [e.g., migration of point defects or dislocations, grain-boundary sliding, grain-boundary (Coble) creep]. These processes are kinematic, and therefore the absorption of energy will be dependent upon the frequency of the propagating wave. As seismic waves in the Earth have a frequency range of mHz to Hz, there is the possibility that the wave speeds and dissipation determined at high frequencies in the laboratory are not relevant to the data obtained from seismic wave measurements of the wave speed and dissipation in the Earth. In this study, the frequency dependence of shear wave speed and dissipation was determined in polycrystalline MgO at seismic frequencies (10 mHz–1 Hz) and temperatures of 20–1300 °C at 200 MPa confining pressure via both torsional forced-oscillation and torsional microcreep measurements at strains less than 10^{-4} and stresses less than 500 kPa.

The study of the velocity and dissipation of seismic waves propagating through $(Mg,Fe)SiO_3$ and $CaSiO_3$ perovskite and magnesio-wüstite is critical to our understanding of seismological models in terms of temperature and composition of the lower mantle. The present study of the viscoelastic rheology of MgO complements the previous determination of the shear wave speed dispersion and dissipation in the $(Mg,Fe)SiO_3$ perovskite analogues $CaTiO_3$ and $SrTiO_3$ by Webb et al. (1999).

Models of the Earth's structure and dynamics rely on measurements of seismic wave dispersion and attenuation. Seismological studies of the shear wave dissipation in the lower mantle calculate a Q^{-1} of 2.8×10^{-3} for depths of 670–2891 km in the Earth (e.g., Durek and Ekström 1995, 1996). Recent seismic frequency-forced oscillation studies have observed Q^{-1} less than 10^{-2} in

polycrystalline materials displaying a frequency-independent shear modulus (Webb et al. 1999; Tan et al. 2001), and higher attenuation was observed as the modulus became frequency-dependent with increasing temperature. Understanding the physical mechanisms producing seismic wave dissipation is therefore of critical importance. Decreases in seismic frequency shear wave speed accompanied by an increase in dissipation can be attributed to an increase in temperature (e.g., Anderson 1980; Budiansky et al. 1983), an increase in defect density (e.g., Karato and Spetzler 1990), the presence of melt (e.g., Budiansky and O'Connell 1980) or a decrease in grain size (e.g., Webb et al. 1999; Tan et al. 2001). The data of Webb et al. (1999) show that a 500 m s^{-1} decrease in shear wave speed (for a 0.1-Hz stress wave) in polycrystalline $CaTiO_3$ perovskite accompanied by an increase in dissipation of half an order of magnitude can be caused by (1) an 800 °C increase in temperature, (2) the presence of ~10 vol% melt or (3) a decrease in grain size from 5 to 0.5 mm.

MgO sample

Sample preparation

The polycrystalline sample was made by hot-pressing MgO powder at 300 MPa and 1300 °C. The 5–50 μm powder supplied by Electronic Space Products International (Ashland, Oregon, USA) was first fired at 1000 °C for 1 h in air and then cold-pressed at 300 MPa into pellets 15 mm in diameter and 10 mm long. The firing resulted in a ~30% reduction in weight due to the loss of CO_2 and H_2O. Five such pellets were then placed in an iron jacket of 0.25-mm wall thickness and hot-pressed at 1300 °C and 300 MPa for 4 h in a gas-charged pressure vessel with argon as the pressure medium. The density of the hot-pressed material was determined by immersion in ethanol to be 97% of the theoretical density of MgO (see Table 1). The weight of the immersed specimen does not change as a function of immersion time in the ethanol. This indicates that the porosity exists as isolated spaces in the sample into which the ethanol cannot flow. Laser-ablation ICP-MS analysis of the sample 20 weeks after it had been removed from its iron jacket showed it had reabsorbed carbon with atmospheric isotopic composition. The presence of carbonate suggests that full densification was impeded by CO_2 gas in the pore spaces at high temperatures.

Sample characterization

Microstructures, phase identification and impurity contents were determined using transmitted and reflected polarized light microscopy (Fig. 1a) and scanning electron microscopy (Fig. 1b; backscattered imaging in a JEOL JSEM6400 instrument). As seen in Fig. 1, the hot-pressed sample is friable, with a large amount of grain-plucking occurring during the cutting and polishing process. The grain size was determined from a thin section of the sample taken after the high-temperature measurements by measuring 1000 linear intercepts along randomly separated lines drawn on micrographs, and multiplying by the geometric factor 1.5 to correct for sectioning effects. The sample had a Gaussian distribution of grain sizes ranging from 15–150 μm, the average grain size being 55 μm with a standard deviation of 26 μm (see Fig. 2). The grain-size distribution was also determined by calculating the volume fraction of grains with a particular diameter using the program StripStar (Heilbronner). The largest

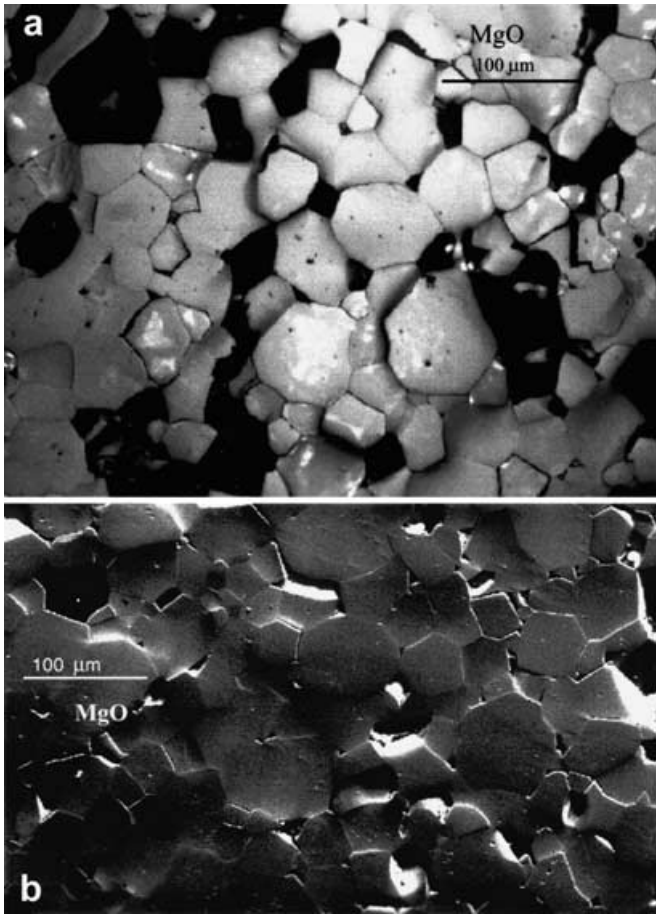

Fig. 1 **a** Light microscope view of the MgO sample after the high-temperature measurements. **b** SEM image of the MgO sample after the high-temperature measurements

Table 1 Shear modulus (at 20 °C) and temperature dependence to 700 °C determined from the forced-oscillation measurements, together with room-temperature ultrasonic determination of wave speeds at ultrasonic frequencies, compared with the high-frequency RPR data of Isaak et al. (1989) (also calculated at 20 °C)

All at 20 °C	G GPa	$\partial G/\partial T$ GPa K^{-1}	ρ g cm^{-3}	v_P m s^{-1}	v_S m s^{-1}	α_v K^{-1}
Present study						
Seismic frequency	116.5 ± 0.5	−0.038 ± 0.001	3.467 ± 0.003	–	5797 ± 13	–
MHz frequencies	120.11 ± 0.2	–	3.467 ± 0.003	9558 ± 8	5886 ± 7	
Isaak et al. (1989)						
MHz frequencies	131.8	−0.026	3.585	9730	6060	3.12×10^{-5} Suzuki (1975)

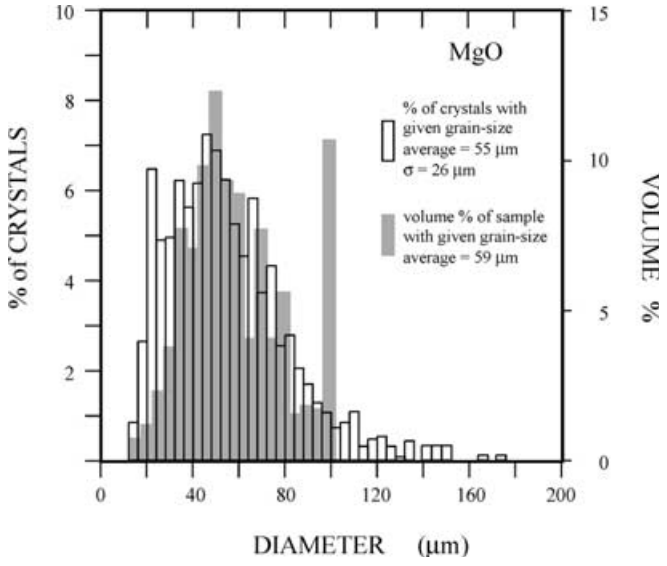

Fig. 2 Grain size calculated from 1000 linear intercepts multiplying the measured lengths by the geometric factor 1.5. The volume fraction occupied by each grain size was calculated using the method of Heilbronner (2000)

volume fraction is made up of 59-μm grains; with a similar contribution to volume by grains larger in diameter than 100 μm (see Fig. 2). (For calculation of the volume fractions for the various grain sizes, it was necessary to truncate the distribution at 100 μm.)

SEM analyses of a polished block prepared from the sample following the mechanical testing revealed isolated domains with a locally high proportion of triple junctions and grain boundaries occupied by forsterite typically containing ~1 wt% CaO. Images of a fracture surface revealed the presence of additional secondary phases – a massive Mg–Ca-bearing phase common in triple-junction tubules and a fibrous material growing within otherwise empty parts of the triple-junction network. These secondary phases are associated with IR absorption peaks for carbonate and brucite, respectively; bulk concentrations of 0.03 wt% CO_2 and ~0.01 wt% H_2O are inferred. Small blebs of Pt (<1 μm) detected within grains and at grain boundaries are interpreted as residual from the MgO manufacturing process. Vacant triple junctions accounting for most of the 3% porosity are commonly bounded by both planar and smoothly curved MgO crystal boundaries.

High-temperature rheology

Microcreep tests

The cylindrical sample used in the microcreep and forced-oscillation measurements was precision-ground from the hot-pressed specimen. The diameter is 11.40 ± 0.02 mm and the length is 30.00 ± 0.01 mm. The ends of the cylindrical sample were polished optically flat and parallel in order to make the best possible mechanical bond between the sample and the similarly polished ends of the Lucalox alumina torsion rods. The cylinder of polycrystalline MgO was wrapped in three layers of 50-μm-thick iron foil (99.95% Fe) and placed between Lucalox alumina torsion rods. A 50-μm-thick foil of iron (99.95% Fe) was used between the ends of the sample and the alumina torsion rods. The entire assembly was then placed in a 0.25-mm-thick mild steel jacket in the torsion apparatus of Jackson and Paterson (1993; see also Jackson 2000).

Torsional microcreep tests to maximum strains of 10^{-4} at maximum stresses of ~100 kPa were performed at high temperature on the sample plus torsion rod assembly. A positive torque of constant amplitude is applied for a fixed time (here typically 1000 s), followed by a period of zero torque application (3000 s). The linearity of the stress/strain/strain-rate behaviour of MgO was demonstrated by determining the modulus and dissipation for a factor of 4 variation in applied torque. The variation in Q^{-1} and G for these different torques at 1000 °C is within the reproducibility of the measurements at the same torque [Q^{-1} ± 15% and G ± 2 GPa].

The microcreep data obtained at temperatures from 400–1300 °C are shown in Fig. 3. The resulting deformation of the sample shows only an instantaneous recoverable elastic component at 400 °C. From 750–1050 °C a time-dependent recoverable (i.e., anelastic) component of deformation accompanies the elastic deformation. Upon removal of the applied torque the time-dependent deformation occurring in this temperature range returns to zero. A non-recoverable (i.e., viscous) component of deformation appears for temperatures of 1100 °C and higher. This is illustrated by the measured time-dependent deformation not returning to zero upon removal of the applied torque.

Forced oscillation measurements

The shear modulus and dissipation were determined as functions of frequency from 10 mHz to 1 Hz by forced torsional oscillation over a temperature range 20–1300 °C at a confining pressure of 200 MPa. The amplitude of the deformation of the sample in response to the application of sinusoidally oscillating shear stress was determined at periods of 1, 3, 8, 15, 28, 54 and 100 s. The phase shift between the applied stress and the resulting strain was also measured. The combination of the amplitudes of stress and strain and the phase shift between them allows the calculation of the viscoelastic response of the material as a function of frequency. The maximum shear stresses and strains experienced by the sample were 0.8 MPa and 10^{-5}, respectively. The shear modulus $G(\omega, T)$, and dissipation $Q^{-1}(\omega, T)$, determined as functions of temperature and frequency, are illustrated in Fig. 4a,b.

The forced-oscillation modulus and dissipation presented in Fig. 4 and discussed here were determined upon staged cooling from 1300 °C. The modulus and attenuation were determined again at 1000 and 1300 °C upon reheating from room temperature. For the same amplitude of applied torque, $Q^{-1}(\omega)$ and $G(\omega)$ determined upon cooling and reheating are reproducible within

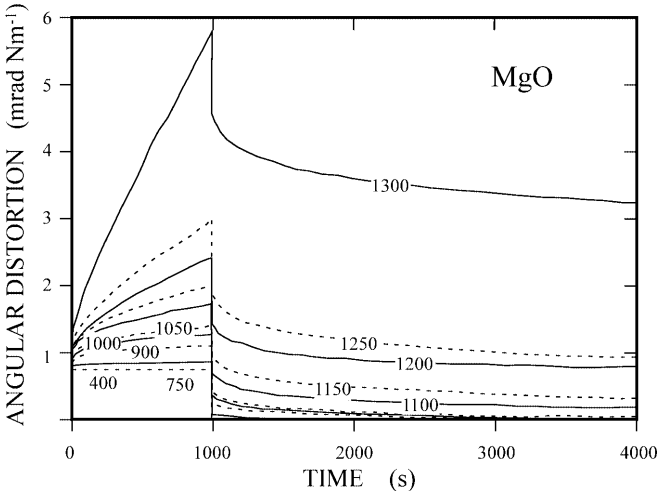

Fig. 3 Angular distortion per unit torque calculated from the micro creep measurements from 400 to 1300 °C

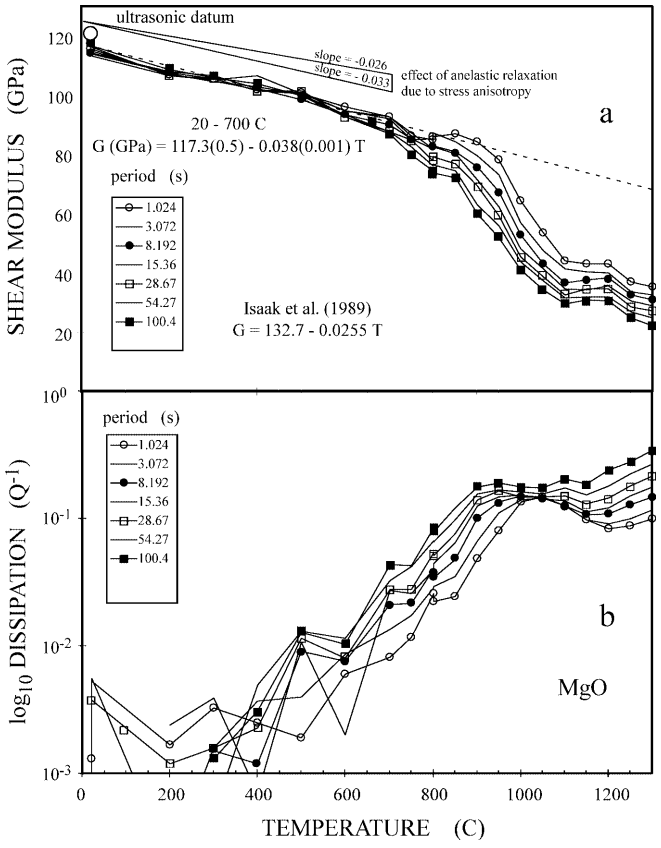

Fig. 4 **a** Frequency-dependent shear modulus of polycrystalline MgO as a function of temperature. The *dashed line* is fit to the data from 20–700 °C. **b** Frequency-dependent shear dissipation of polycrystalline MgO as a function of temperature

the experimental uncertainties given above. The reproducibility of the modulus and dissipation at 1300 °C over the 80-h exposure to temperatures above 1000 °C is taken to indicate that no mechanically significant microstructural evolution occurred over the duration of the measurements. The thin section of the sample after the high-temperature torsion measurements showed the absence of a significant population of grains <5 μm, which were present in the sample before the high-temperature measurements (not seen in Fig. 2, which is for the specimen after mechanical testing). The continued growth of these small grains during the time at high temperature while the forced-oscillation and microcreep measurements were being performed does not appear to affect (within error) the measured frequency- and time-dependent rheology.

Ultrasonic measurements

The compressional and shear wave velocities have been determined on this MgO sample at ambient conditions using ultrasonic (40 MHz) phase comparison techniques (Webb et al. 1999). An ~8-mm-long piece was cut from the sample after the torsion measurements. The ends of this short cylinder were cut parallel to each other, and polished flat. The measurements were performed by glueing (with phthalic anhydride) the sample to a 10-mm-long steel buffer rod to which a lithium niobate transducer had been glued (using Crystal Bond). The ultrasonic velocities were determined to be $v_P = 9.558 \pm 0.008$ km s^{-1} and $v_S = 5.886 \pm 0.007$ km s^{-1}.

Data analysis

The Andrade model was used to fit the forced-oscillation and the microcreep data. The Andrade model of linear viscoelasticity describes time evolution of strain as a function of constant applied stress [$\varepsilon(t) = J(t)\sigma$] by the empirical creep function

$$J(t) = J_u + \beta t^n + t/\eta \quad (1/3 \leq n \leq 1/2) \tag{1}$$

with instantaneous elastic shear compliance J_u, which is the inverse of the unrelaxed shear modulus G, time t, the parameter β describing the magnitude of the transient deformation, and the steady-state Newtonian viscosity η. The strain [$\varepsilon(t) = \varepsilon_0 \exp i(\omega t - \delta)$] response to a sinusoidally varying stress [$\sigma(t) = \sigma_0 \exp(i\omega t)$] as a function of time can be calculated from the creep function by superposition of the responses to a series of step function stresses assuming linear stress–strain behaviour (see Nowick and Berry 1972). The resulting expression for the dynamic compliance $J^*(\omega) = \varepsilon(t)/\sigma(t)$ for the Andrade model is

$$J^*(\omega) = J_u + \beta\Gamma(1+n)(i\omega)^{-n} - i/\eta\omega = J_1(\omega) - iJ_2(\omega) \ , \tag{2}$$

where $\Gamma(x)$ is the Gamma function (Findley et al. 1976; Gribb and Cooper 1998; Jackson 2000). It is clear from Eqs. (1) and (2) that the creep and forced oscillation data provide the same information about the mechanical behaviour of materials.

The frequency-dependent shear modulus is calculated from the real and imaginary parts of the dynamic compliance:

$$G^*(\omega) = \frac{J_1(\omega) - iJ_2(\omega)}{J_1^2(\omega) + J_2^2(\omega)} \ . \tag{3}$$

The strain energy dissipation Q^{-1} is the ratio of the imaginary and real parts of the dynamic compliance:

$$Q^{-1}(\omega) = \frac{J_2(\omega)}{J_1(\omega)} \ , \tag{4}$$

and its negative logarithmic frequency derivative is

$$\alpha = -\frac{\partial \ln[Q^{-1}(\omega)]}{\partial \ln[\omega]} \ . \tag{5}$$

Measurements are conducted on specimen-bearing and reference assemblies which are identical in every respect except for the replacement of the specimen by a dummy made from high-grade Lucalox (General Electric) polycrystalline alumina. Subtraction of the torsional compliance of the reference assembly from that for the specimen assembly eliminates the unwanted contribution from the Lucalox alumina torsion rods. This difference is the contrast in torsional compliance between the jacketed specimen and the jacketed Lucalox dummy. This is converted into an absolute determination of the torsional compliance of the specimen itself by treating the behaviour of the alumina as elastic and using prior forced-oscillation results describing the complex modulus of the iron jacket material. In the case of the forced-oscillation data, these calculations are done at each period of measurement. In the case of the microcreep data, these calculations are done by fitting an Andrade equation (with $n = 1/3$) separately to the microcreep data for each of the specimen and reference assemblies. The difference between the Laplace transforms of these creep functions, which is the frequency-dependent dynamic compliance of the jacketed specimen relative to the jacketed alumina dummy specimen, is calculated, and thereafter the analysis proceeds as for the forced-oscillation data. Finally, the variation of both shear modulus and dissipation with period, inferred from either forced-oscillation or microcreep data, is fitted to the Andrade model (Jackson 2000; Fig. 5).

The Andrade model fits the forced-oscillation and microcreep data above 1100 °C listed in Table 2. At temperatures below 1100 °C, the response of the specimen is anelastic – meaning that the steady-state viscosity η is effectively infinite. Constraining the value of J_u to be the extrapolated high-temperature ultrasonic value resulted in fits with a χ^2 value at least twice those obtained by

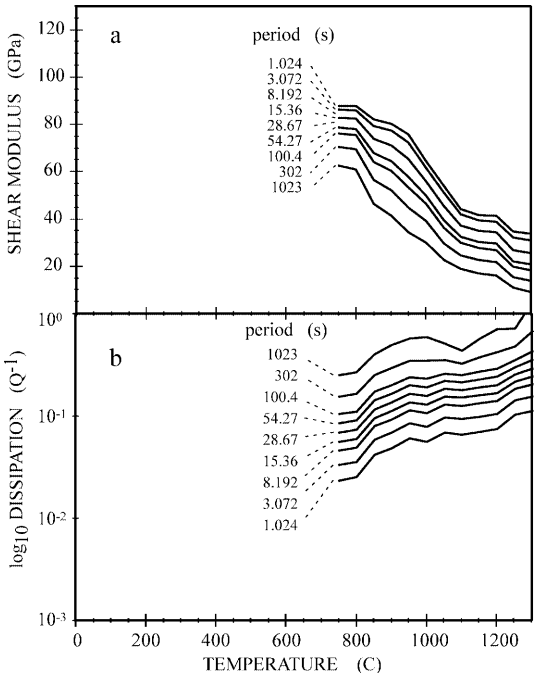

Fig. 5 The shear modulus (**a**) and dissipation (**b**) as a function of temperature determined from the microcreep measurements. The data have been recalculated in frequency space

allowing J_u to be unconstrained. As the best description of the forced-oscillation and microcreep data is obtained by unconstrained values of J_u, these are the fits presented here.

Temperature-dependent rheology

The transition from elastic to viscoelastic behaviour

There is excellent agreement between values of shear modulus determined by forced-oscillation and microcreep measurements with respect to both the magnitude of the modulus and the details of its temperature dependence, including the presence of the $G(T)$ plateau at 1100–1200 °C (cf. Figs. 4a and 5a). While there is relatively good agreement in the magnitude of the dissipation determined from the forced-oscillation and microcreep data, the dissipation maximum most clearly resolved for short periods at ~1050 °C is not seen in the microcreep data. The disagreement between the microcreep and forced-oscillation dissipation data is due to the lack of resolution of the microcreep data at short time scales, where the forced-oscillation data are preferred.

Together, the forced-oscillation and microcreep data reveal dramatic changes in the rheological behaviour of MgO across the 20–1300 °C temperature range. For temperatures of 20–700 °C the shear modulus determined from the forced-oscillation data is almost frequency-independent and can be described as a linear function of temperature with $G_{T=20\,^\circ C} = 116.5 \pm 0.5$ GPa and $\delta G/\delta T = -0.038 \pm 0.001$ GPa K^{-1}. The values of Q^{-1} are low (generally $< 10^{-2}$) and scattered. The microcreep data indicate fully recoverable time-independent (elastic) deformation of MgO at 400 °C.

For temperatures > 700 °C the behaviour deviates markedly from the elastic ideal with appreciable dissipation and associated frequency dependence of the shear modulus. The parameter $\alpha = \partial \ln Q^{-1}/\partial \ln T_{osc}$, a measure of the strength of the frequency (or period) dependence of the dissipation, varies systematically with temperature across the interval 700–1300 °C (Fig. 6). At the highest temperatures (1200–1300 °C), the frequency dependence of the dissipation is well described by a power law with an exponent α of 0.27. The generally higher (lower) values of α for the temperature intervals 700–900 °C (950–1150 °C) result from the progressive movement of a broad $Q^{-1}(T_{osc}, T)$ peak from periods longer than 100 s ($T < 900$ °C) across the 1–100 s observational "window" to periods shorter than 1 s ($T > 1300$ °C). Thus the nearly frequency-independent Q^{-1} at 1000 and 1050 °C is the result of approximate cancellation between the contributions from the monotonic "background" and from the long-period side of the dissipation peak. The observation that appreciable irrecoverable deformation occurs only for temperatures $T \geq 1100$ °C (Fig. 3) indicates that the broad dissipation peak is associated with recoverable (anelastic) behaviour.

Viscosity

At temperatures above 1050 °C, the steady-state viscosity is well resolved especially by the microcreep data, all of which were obtained over intervals of 1000 s of torque application (Fig. 7). Systematically lower and more scattered viscosities are inferred from the forced-oscillation data obtained for periods of 1–100 s. The values derived from the microcreep and forced-oscillation data are most consistent at the highest temperatures where the viscosity is lowest and the Maxwell time $\tau = \eta J_U$ is either less than or not much greater than 100 s (see Table 2). The viscosities associated with the

Table 2 Parameters for Andrade model fits to the forced oscillation (fto) and micro creep (crp) data

T °C	J_u 10^{-3} GPa^{-1}	n	β 10^{-3}	η 10^{12} Pa s	$\tau(=\eta J_u)$ s	χ^2
1100						
fto	23.5 ± 8.2	0.09 ± 0.03	25.2 ± 8.3	8.5 ± 3.8	200	14.1
crp	20.2 ± 0.4	0.36 ± 0.01	6.1 ± 0.4	44.3 ± 33.8	894	0.1
1150						
fto	10.2 ± 5.1	0.11 ± 0.04	17.1 ± 5.2	8.9 ± 9.7	91	25.2
crp	20.9 ± 0.5	0.34 ± 0.02	7.0 ± 0.5	16.4 ± 5.4	343	0.1
1200						
fto	17.5 ± 1.6	0.20 ± 0.04	9.5 ± 1.6	6.5 ± 2.6	114	8.5
crp	20.9 ± 0.5	0.33 ± 0.02	7.6 ± 0.5	10.8 ± 2.4	225	2.5
1250						
fto	22.2 ± 1.2	0.26 ± 0.04	9.7 ± 1.3	4.5 ± 1.9	101	10.9
crp	23.3 ± 0.7	0.34 ± 0.02	12.5 ± 0.7	9.8 ± 3.0	228	3.9
1300						
fto	23.7 ± 1.1	0.31 ± 0.04	9.7 ± 1.1	2.9 ± 1.0	68	6.6
crp	23.6 ± 0.8	0.33 ± 0.02	13.9 ± 0.8	3.9 ± 0.5	92	11.6

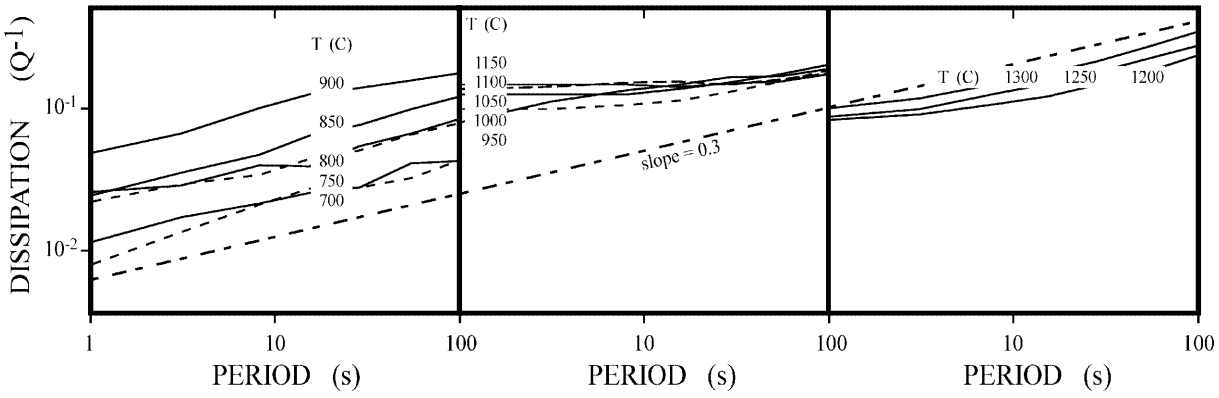

Fig. 6 Dissipation (Q^{-1}) from the forced oscillation measurements as a function of wave period

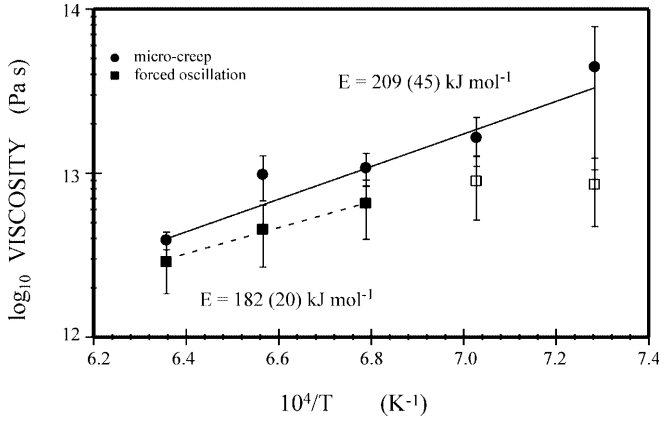

Fig. 7 Viscosity calculated from Andrade model fits to the forced oscillation and microcreep data plotted as a function of inverse temperature. The *empty symbols* indicate forced-oscillation data not used in the calculation of activation energy. The relaxation times at these temperatures are greater than the longest-period sinusoidal shear stress wave (100 s)

Andrade model fit to the microcreep data constrain the Arrhenian activation energy E_v for viscous flow in the temperature range 1100–1300 °C to be 209 ± 45 [2σ] kJ mol^{-1}.

Discussion

MHz vs. seismic frequency data

At room temperature the shear modulus calculated from the shear wave speed measured ultrasonically under bench-top conditions is consistent, within the mutual uncertainties, with that calculated from the 200 MPa forced-oscillation data (Table 1). Such consistency excludes the possibility of the strong pressure dependence that would be expected of pressure-induced crack closure. It is therefore concluded that the crack porosity must be very low. Furthermore, the *P* and *S* wave speeds of the present sample on the bench top are 97–98% of the values expected for a zero-porosity polycrystalline sample (Table 1). The 2–3% deficit in wave speed is reasonable for a fine-grained hot-pressed material with 3% (sub-equant) porosity (Kung et al. 2000).

In Fig. 4a the temperature dependence of the shear modulus determined by forced oscillation at seismic frequencies is compared with that calculated for polycrystalline MgO from the high-frequency single-crystal elasticity data of Isaak et al. (1989). For the temperature range 20–700 °C, the seismic frequency data are offset to systematically lower values as the result of porosity (discussion above) and also reveal a value of $|dG/dT|$, which is 50% larger than that inferred from the high-frequency measurements (see Table 1). A straight-line fit over a smaller temperature range does not reduce the temperature dependence of the modulus. The greater value of $|dG/dT|$ observed in the present study, along with non-zero values of dissipation (Fig. 4b), must reflect a modest amount of anelastic relaxation concentrated in the upper half of the 20–700 °C temperature range.

Anelastic and viscoelastic relaxation

MgO remains cubic at all temperatures below the melting point (~2800 °C). The onset of markedly frequency-dependent modulus and intense strain-energy dissipation observed above 700 °C in this material cannot therefore be attributed either to phase transitions or to melting. An explanation of the anelastic (700–1050 °C) and viscous (1100–1300 °C) behaviour of this polycrystalline material is therefore sought in thermally activated solid-state deformation mechanisms.

Anelastic relaxation of the internal stresses caused by the elastic anisotropy of the individual crystallites within a stressed polycrystalline material is thought to account for reduction of the shear modulus from the unrelaxed Hashin–Shtrikman average G_{HS} to the Reuss (uniform strain) lower bound G_R with increasing temperature (Jackson et al. 2000). The elastic anisotropy for MgO increases with increasing temperature causing $\Delta G/G_U = (G_{HS} - G_R)/G_{HS}$ to increase appreciably from 0.02 at room temperature to 0.06 at 1050 °C (Isaak et al. 1989). Complete relaxation of the intergranular stresses arising in the polycrystal from the elastic

anisotropy of individual crystallites would accordingly result in a substantially larger average value of $|dG/dT|$ (0.033 GPa K^{-1}) at low frequencies than is inferred at high frequencies (0.026 GPa K^{-1}) (see Fig. 4a). This process is probably partly responsible for the higher value of $|dG/dT|$ measured at seismic frequencies and temperatures of 20–700 °C in the present study. However, an additional explanation is clearly required for the much greater degree of modulus relaxation observed at higher temperatures (Fig. 4a).

Anelastic relaxation in fine-grained materials may also arise from viscous grain-boundary sliding accommodated by elastic deformation of the neighbouring grains. There are a number of different models for the resulting relaxation of the shear modulus (see Jackson et al. 2000 for a full discussion). Raj and Ashby (1971) obtained a relationship for elastically accommodated grain-boundary sliding in a two-dimensional model polycrystal comprised of hexagonal crystallites whereby

$$\frac{G_{\text{relax}}}{G_{\text{unrelax}}} = \frac{1}{1 + 0.57(1 - \nu)} \quad . \tag{6}$$

This relationship yields a $\Delta G/G_u$ [$=(G_{\text{unrelaxed}}-G_{\text{relaxed}})/G_{\text{unrelaxed}}$] value of 0.31 at 1050 °C for MgO, which has a Poisson's ratio $\nu = 0.2$ at this temperature. Therefore, much of the 57% anelastic relaxation of the shear modulus observed at 1050 °C could plausibly be the result of elastically accommodated grain-boundary sliding (possibly facilitated by the presence of a small amount of an interstitial H_2O–CO_2-rich fluid phase).

Equation (7) was used to fit the frequency and temperature dependence of attenuation in both the anelastic and viscoelastic regimes.

$$Q^{-1}(\omega, T) = Q_0^{-1}\omega^{-\alpha}\exp\left(\frac{-\alpha E}{RT}\right) \quad . \tag{7}$$

Figure 8 shows that the activation energy for dissipation is the same for the anelastic (251 ± 36 kJ mol^{-1} [2σ]) and viscoelastic (250 ± 38 kJ mol^{-1}) regimes, and that the frequency dependence for the anelastic (0.30 ± 0.02) and viscoelastic (0.27 ± 0.01) attenuation is also the same. This suggests that the same underlying deformation mechanism is involved in these two different rheologies. This activation energy value is comparable with that associated with the viscosity inferred from the Andrade fits to the microcreep data (209 ± 45 kJ mol^{-1}; Fig. 7). The activation energies for extrinsic lattice diffusion in mildly impure MgO are 266 kJ mol^{-1} for Mg and 261 kJ mol^{-1} for O (Frost and Ashby 1982). Somewhat lower activation energies have been calculated for extrinsic diffusion of Mg (191 kJ mol^{-1}) and O (193 kJ mol^{-1}) (Vocadlo et al. 1995). Activation energies slightly lower than those measured for lattice diffusion have been inferred for grain-boundary diffusion in MgO: 230 kJ mol^{-1} for O and ~200 kJ mol^{-1} for Mg (Frost and Ashby 1982). These are indistinguishable from the activation energies inferred for the dissipation background and steady-state viscosity in the present study, supporting the view that grain-boundary diffusion plays an important role. However, it should be noted that the background dissipation measured by Getting et al. (1997) for shear deformation of single-crystal MgO, similarly modelled, has an activation energy of 233 ± 50 kJ mol^{-1}, presumably reflecting diffusional control of the stress-induced migration of dislocations.

It is possible that the wide distribution of grain sizes (15–150 μm) in this sample is responsible for the persistence to relatively high temperatures of elastic accommodation for grain-boundary sliding. If the grains were deformed viscously by a mechanism which depended upon grain size (i.e., diffusional creep), at a constant temperature and period of applied torque, a restoring force for the viscous deformation of the smaller grains would be provided by the elastic deformation of the larger grains. This would result in

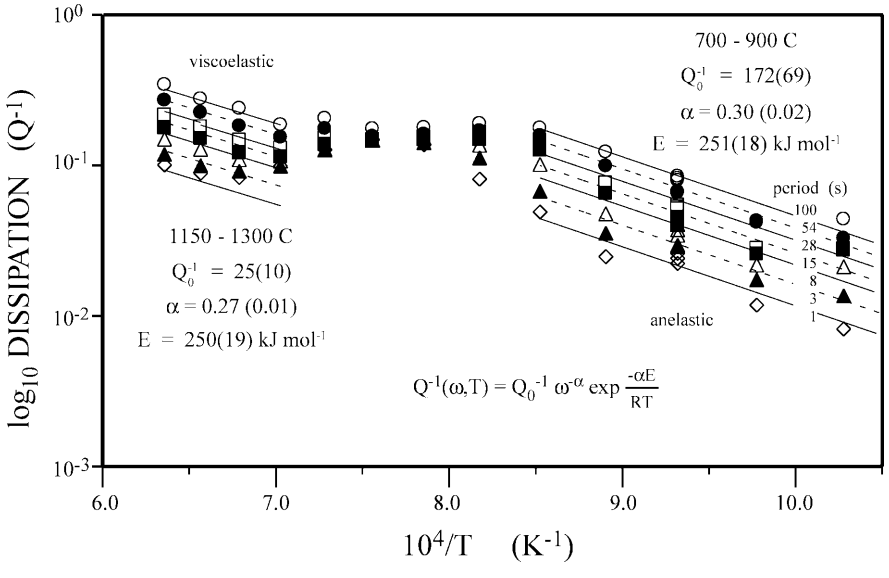

Fig. 8 Forced oscillation dissipation as a function of inverse temperature

macroscopic anelastic behaviour. At some higher temperature, the viscosity would be low enough to allow appreciable permanent deformation even of the largest grains, resulting in viscous deformation of the entire sample. If this were the mechanism by which the anelastic and viscous regimes of deformation occurred in the present MgO sample, the lowest temperature at which appreciable anelastic deformation is observed (750 °C) would be that at which the smallest grains (15 μm) deformed viscously, and the temperature for the onset of viscous deformation of the sample (1050 °C) would be that at which the largest grains (150 μm) deformed viscously (see Fig. 9). This scenario requires a balance between the temperature and grain-size sensitivities for diffusional creep such that reduction of grain size from 150 to 15 μm has the same impact upon viscosity as a temperature increase from 750 to 1050 °C.

With

$$\eta = \frac{\sigma}{\dot{\varepsilon}} = \mathrm{A} d^n \exp\left(\frac{E}{RT}\right) \quad n = 2, 3 \tag{8}$$

(e.g., Frost and Ashby 1982), we thus require that

$$\Delta \log_{10} \eta = n \Delta \log_{10} d = \frac{E}{2.303R} \Delta\left(\frac{1}{T}\right) \ , \tag{9}$$

yielding for the activation energy

$$E = 2.303 nR \frac{\Delta \log_{10} d}{\Delta\left(\frac{1}{T}\right)} \quad . \tag{10}$$

If the viscous deformation is achieved by Nabarro–Herring (lattice diffusion) creep, the grain-size dependence of deformation is d^2, and the activation energy inferred from Eq. (10) is ~173 kJ mol^{-1}. If the viscous deformation is achieved by Coble (grain-boundary diffusion) creep, the grain-size dependence of deformation is d^3, and the calculated activation energy is ~259 kJ mol^{-1}. That these calculated activation energies are comparable with the range of activation energies considered above adds some credence to the notion that the range of grain sizes is influential in maintaining elastic accommodation at moderate temperatures in this material.

Viscosity and diffusivity

The grain size (15–150 μm) – normalized stress ($\sigma/G \sim 10^{-6}$) - temperature ($\leq$ 1300 °C) regime of these measurements plots within the field for diffusionally accommodated grain-boundary sliding on the steady-state deformation mechanism maps for MgO presented by Frost and Ashby (1982). These authors infer that grain-boundary diffusion of oxygen is likely to be rate-limiting. If the steady-state viscosities inferred from the microcreep tests of the present study are attributed to diffusion-accommodated grain boundary sliding, an effective diffusivity D_{eff} can be calculated from the inferred viscosity through the left-hand side of the following equation of Raj and Ashby (1971):

$$D_{\mathrm{eff}} = \frac{RTd^2}{B\Omega\eta} = D_\ell \left[1 + \frac{\pi\delta}{d}\frac{D_\mathrm{b}}{D_\ell}\right] \ , \tag{11}$$

with viscosity $\eta = \sigma/\dot{\varepsilon}$, temperature T(K), grain diameter d, $B = 42$, and molar volume $\Omega = 11.246 \times 10^{-6}$ m^3 for MgO. The values of D_{eff} (T) thus calculated for a grain size of 55 μm and for grain sizes differing by a factor of 3 are represented by the solid lines in Fig. 10. On the right-hand side of this equation is the relationship between D_{eff} and the lattice diffusivity D_ℓ, the

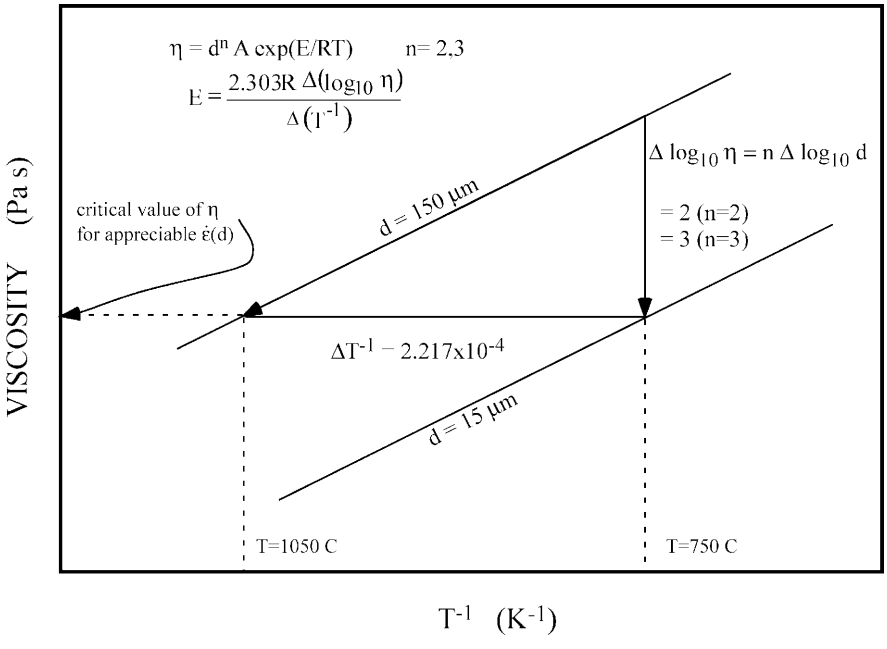

Fig. 9 Estimation of the activation energy for the mechanism by which the grain-size-dependent anelastic and viscoelastic rheology occurs

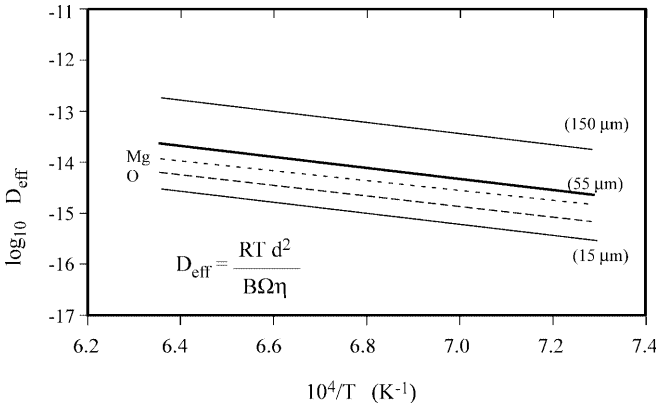

Fig. 10 Diffusivity calculated from the Andrade model fit to the combined forced-oscillation (1200–1300 °C) and microcreep (1100–1300 °C) viscosity data compared with the calculations of Vocadlo et al. (1995). An extrinsic defect concentration of 0.1 is required to match the modelled and calculated D_{eff}

boundary diffusivity D_b and the thickness δ of the grain boundary.

For comparison, the lattice diffusivities for Mg and O calculated from the results of Vocadlo et al. (1995; activation energies of 191 kJ mol^{-1} for Mg and 193 kJ mol^{-1} for O diffusion) for the high defect concentration of 10^{-1} are plotted in Fig. 10 as broken lines. If the diffusional accommodation of the grain-boundary sliding were to be accomplished by lattice diffusion, then very high defect concentrations would clearly be required. A more attractive alternative is to propose diffusional accommodation by grain-boundary diffusion, consistent with the deformation mechanism maps of Frost and Ashby (1982). Under these circumstances the term in parentheses on the right-hand side of Eq. (11), which is a function of the ratio of grain-boundary diffusivity D_b and lattice diffusivity D_ℓ, may be $\gg 1$, allowing the inferred effective diffusivity to be matched with much lower lattice defect concentrations. Control of the steady-state viscosity by boundary diffusion derives additional support from the fact that activation energy (preferred value 209 ± 45 kJ mol^{-1}) compares more favourably with those for grain-boundary diffusion than with the values for extrinsic lattice diffusion (see discussion of activation energies above).

Conclusion

The forced-oscillation and the microcreep data provide consistent information about the elastic, anelastic and viscous deformation of the polycrystalline MgO sample. The deformation appears to be adequately described by linear viscoelastic theory. The grain-size/stress/temperature regime of these measurements plots within the diffusion creep regime for MgO tabulated by Frost and Ashby (1982). Although the forced-oscillation and microcreep measurements result in identical values of shear modulus as a function of temperature and period, the microcreep measurements do not show the anomalous frequency-dependent values of dissipation determined in the forced-oscillation measurements at ~1050 °C. This is due to the lack of resolution in the microcreep data at short time scales. The forced-oscillation data, however, do not illustrate the change from anelasticity to viscoelasticity with increasing temperature, which the microcreep measurements document so clearly.

The activation energies for anelastic and viscoelastic deformation are identical and agree with the activation energies of Mg and O diffusion. Therefore, it appears that the two types of rheological behaviour observed in the present polycrystalline sample are due to diffusive creep with the anelastic behaviour due to diffusive slip of a segment of a grain boundary accommodated by elastic distortion of unslipped regions of the grain boundary.

The dissipation measured for this fine-grained 55 ± 26 μm MgO sample at 1300 °C ranges from 10^{-1} to 10^{0} for seismic frequencies (see Figs. 4 and 5). This dissipation is the same order of magnitude as that measured by Webb et al. (1999) for fine-grained $CaTiO_3$ (3–20 μm) and $SrTiO_3$ (8 μm) analogues of $MgSiO_3$ perovskite. This suggests that the measured shear wave dissipation of the lower mantle (Q^{-1} of 2.8×10^{-3} e.g., Durek and Ekström 1995, 1996) can be accommodated by diffusional processes in a perovskite + magnesiowüstite mantle with a grainsize of 5–50 mm. These diffusional processes may result in either anelastic or viscous deformation of the Earth. Although it was not resolvable from the present data, an anelastic deformation process would result in a high Q^{-1} being observed over a specific band of seismic frequencies with lower dissipation values determined for frequencies outside this band.

Acknowledgments Samples were precision-ground by Andrew Wilson, and polished sections prepared by Harri Kokkonen, who also did the SEM work. Uli Faul calculated the volume fraction of grain sizes. The density measurements were done by Lara Weston.

References

Anderson DL (1980) Bulk attenuation in the Earth and viscosity of the core. Nature 285: 204–207

Budiansky B, O'Connell RJ (1980) Bulk dissipation in a heterogeneous material. In: Nemat–Nasser S (ed) Solid earth geophysics and geotechnology. American Society for Mechanical Engineering, New York, pp 1–10

Budiansky B, Sumner EE, O'Connell RJ (1983) Bulk thermoelastic attenuation of composite materials. J Geophys Res 10: 10343–10348

Durek JJ, Ekstrom G (1995) Evidence of bulk attenuation in the asthenosphere from recordings of the Bolivia earthquake. Geophys Res Lett 2: 2309–2312

Durek JJ, Ekström G (1996) A radial model of anelasticity consistent with long-period surface-wave attenuation. Bull Seism Soc Am 86: 144–158

Findley WN, Lai JS, Onaran K (1976) Creep and relaxation of non-linear viscoelastic materials. North Holland, Amsterdam, 367 pp

Frost HJ, Ashby MF (1982) Deformation-mechanism maps. The plasticity and creep of metals and ceramics. Pergamon, New York, 166 pp

Getting IC, Dutton SJ, Burnley P, Karato S-I, Spetzler HA (1997) Shear attenuation and dispersion in MgO. Phys Earth Planet Int 99: 249–257

Gribb TT, Cooper RF (1998) Low-frequency shear attenuation in polycrystalline olivine: grain-boundary diffusion and the physical significance of the Andrade model for viscoelastic rheology. J Geophys Res 103: 27267–27279

Heilbronner, R (2000) www.unibas.ch/earth/micro/downloads/downloads.html

Isaak DG, Anderson OL, Goto T (1989) Measured elastic moduli of single-crystal MgO up to 1800 K. Phys Chem Miner 16: 704–713

Jackson I (2000) Laboratory measurement of seismic wave dispersion and attenuation: recent progress. In: Karato S-I, Forte AM, Liebermann RC, Masters G, Stixrude L (eds) Earth's deep interior: mineral physics and tomography from the atomic to the global scale. Geophysical Monograph 117, American Geophysical Union, Washington, DC, United States, pp 265–289

Jackson I, Fitz Gerald JD, Kokkonen H (2000) High-temperature viscoelastic relaxation in iron and its implications for the shear modulus and attenuation of the Earth's inner core. J Geophys Res 105: 23605–23634

Jackson I, Paterson MS (1993) A high-pressure, high-temperature apparatus for studies of seismic wave dispersion and attenuation. PAGEOPH 141: 445–466

Karato S, Spetzler HA (1990) Defect microdynamics in minerals and solid-state mechanisms of seismic wave attenuation and velocity dispersion in the mantle. Rev Geophys 28: 399–421

Kung J, Rigden S, Gwanmesia G (2000) Elasticity of $ScAlO_3$ at high pressure. Phys Earth Planet Int 118: 65–75

Nowick AS, Berry BS (1972) Anelastic relaxation in crystalline solids. Academic Press, New York, 677 pp

Raj R, Ashby MF (1971) On grain-boundary sliding and diffusional creep. Metallurg Trans 2: 1113–1127

Suzuki I (1975) Thermal expansion of periclase and olivine, and their anharmonic properties. J Phys Earth 23: 145–159

Tan BH, Jackson I, Fitz Gerald JD (2001) High-temperature viscoelasticity of fine-grained polycrystalline olivine. Phys Chem Mineral 28: 641–664

Vocadlo L, Wall A, Parker SC, Price GD (1995) Absolute ionic diffusion in MgO – computer calculations via lattice dynamics. Phys Earth Planet Int 88: 193–210

Webb SL, Jackson I, Fitz Gerald J (1999) Viscoelasticity of the titanate perovskites $CaTiO_3$ and $SrTiO_3$ at high temperature. Phys Earth Planet Int 115: 259–291